Structures 49 (2023) 58–69

Contents lists available at ScienceDirect

Structures

journal homepage: www.elsevier.com/locate/structures

Nonlinear static analysis of extreme structural behavior: Overcoming convergence issues via an unconditionally stable explicit dynamic approach

Si-Cong Xie [a,b], Chinmoy Kolay [c], De-Cheng Feng [a,*], James M. Ricles [d]

[a] Key Laboratory of Concrete and Prestressed Concrete Structures of the Ministry of Education, Southeast University, Nanjing, 211189, China
[b] Department of Civil and Environmental Engineering, Politecnico di Milano, Milano, 20133, Italy
[c] Department of Civil Engineering, Indian Institute of Technology Kanpur, Kanpur, 208016, India
[d] Department of Civil and Environmental Engineering, Lehigh University, Address Two, Bethlehem, PA 18015, USA

ARTICLE INFO

Keywords:
Extreme behavior
Convergence problem
Direct explicit integration algorithm
Multi-support excitation
Unconditionally stable

ABSTRACT

Simulating extreme structural behavior is of vital importance as it is a major means to study the damage and failure mechanism of engineering structures. However, convergence issues frequently occur when simulating structural response under extreme loading using traditional nonlinear solution strategies, e.g., the Newton–Raphson family of methods. Though commercial finite element software provides explicit dynamic methods to overcome this issue, they are only conditionally stable and require a small time step size. In this paper, a new explicit dynamic approach to simulate static problems involving extreme structural behavior is presented. The multi-support excitation pattern is employed to apply a nodal displacement history of the problem in a dynamic way, then the unconditionally stable explicit KR-α method is used to eliminate the convergence issues. Three examples are presented to illustrate the effectiveness of the proposed dynamic approach, and a parametric study is conducted to investigate the influence of the algorithmic parameters. The results indicate that the proposed method provides the same accuracy as the traditional static method without any convergence issues.

1. Introduction

The finite element method (FEM) is a common way to study the damage and failure of reinforced concrete (RC) structures, especially, nonlinear static analysis is preferred as it can reproduce the whole process of the damage evolution and reveal the failure mechanism. However, since structural failure usually involves extreme behavior, e.g., rebar buckling and concrete crushing, it can be difficult to accurately and effectively perform and analyze since the stress state is complicated. Furthermore, extreme behavior generally occurs suddenly, and thus convergence problems can be encountered. The model may fail before the structure reaches its real limit state, thus sufficient information about the failure mechanism cannot be obtained.

In order to overcome the convergence issue in static nonlinear extreme behavior modeling, several approaches have been developed in the last few decades. To name a few, the arc-length method is proposed to perform buckling analysis instead of using load-control schemes [1]. The line search technique is developed to improve the direction search in nonlinear iterations when using full and modified Newton–Raphson methods [2]. To solve problems with both material and geometrical nonlinearities, the Krylov–Newton Accelerations method is used to improve the convergence [3]. Also, the quasi-Newton method with BFGS-type secant stiffness operator was developed by researchers for the cyclic loading analysis of concrete structures [4,5]. However, these methods can only improve the convergence problem rather than eliminating the issue. It is still a challenging task to model extreme behavior, especially in the assessment of structures subjected to complex stress states (e.g., shear effect).

Another way to deal with the convergence issue in static extreme behavior modeling is to employ dynamic direct integration algorithms, especially the explicit family ones. In fact, in modeling structures made of brittle materials such as masonry and concrete, unstable nonlinearities due to crack propagation and/or strain-softening usually exist and may induce local dynamic processes in the middle of an overall static process under certain conditions, and dynamic algorithms may be more suitable to deal with such unstable nonlinearities [6]. Several dynamic solution methods have been applied to solve static problems, and examples include buckling analysis involving mode jumping [1] and snap-through [7], crack propagation simulation in RC [8,9] and masonry structures [10], debonding failure analysis in FRP-strengthened beams under static loads [6], in-plane behavior simulation of masonry infilled concrete frames [11] and loading–unloading–reloading behaviors simulation of RC beams [12]. However, these applications are

* Corresponding author.
E-mail address: dcfeng@seu.edu.cn (D.-C. Feng).

https://doi.org/10.1016/j.istruc.2023.01.086
Received 3 August 2022; Received in revised form 13 December 2022; Accepted 15 January 2023

usually based on commercial FEM software like ABAQUS, in which traditional conditionally stable explicit algorithms (e.g., central difference method) are employed. To keep the stability of the dynamic algorithm, a strict limitation is required in the time step size, usually at the level of 10^{-6} s, which represents a great computational cost [13]. In addition, as an open-source FEM software, OpenSees is widely used in various structural analysis but no one has employed the dynamic integration algorithms to solve the convergency issue involving in static extreme behavior simulations. In fact, convergency issues occur frequently in OpenSees especially for structures under complicated stress states such as shear walls under cyclic loadings.

In general, dynamic direct integration algorithms can be divided into two categories: the implicit family and the explicit family. The implicit algorithms are unconditionally stable, such as the Newmark-β method [14] and the generalized-α method [15]. These implicit algorithms require forming the tangent stiffness matrix at each time step and the utilization of an iteration scheme to satisfy equilibrium at the current time step. Therefore, convergence issues may occur when forming the tangent stiffness matrix under nonlinear scenarios. One solution to avoid the convergence issue is to utilize explicit algorithms in which no tangent stiffness matrix and no iteration are required, such as the widely-used central difference method(CDM). However, the CDM is only conditionally stable and requires a time step size that is inversely proportional to the highest natural frequency of the structure, which is usually unacceptable for a system with a large number of freedoms. Moreover, the CDM is a non-dissipative scheme, the solution accuracy can be severely ruined by spurious oscillations which are caused by the dispersion errors in the high-frequency modes. To avoid the extremely small time step size, some unconditional stable explicit methods are proposed, such as Chang's algorithm [16] and CR algorithm [17]. However, Chang's algorithm is only explicit for displacement and becomes implicit for systems with velocity-dependent nonlinear responses [18], and CR algorithm will encounter adverse overshoot response in high-frequency modes [19]. To avoid spurious oscillations, methods with controllable numerical damping are proposed, such as the Bathe method [20]. Bathe method adopted a substeps technique and this technique can be applied to both explicit [20] and implicit algorithms [21–23]. Although Bathe's explicit algorithm achieved desired numerical damping to suppress spurious oscillations of high frequencies and an extended stability limit compared to the CDM, it is still a conditionally stable algorithm. Recently, a set of unconditionally stable explicit algorithms with controllable numerical damping has been proposed [24–28]. The KR-α method is one such family of algorithms which has been implemented in the FEM software OpenSees. The method has been already used in various numerical simulations, e.g., progressive collapse simulation of RC structures [29] and in real-time hybrid simulations [30]. The KR-α method can be also used in nonlinear static analysis involving extreme structural behavior, which paves the way for this study.

The aim of this paper is to use the dynamic KR-α method in simulation of static extreme structural behavior through the OpenSees platform [31]. The formulation of the KR-α method is firstly derived, and the application of the nodal displacement to any arbitrary set of nodes through the `multi-support excitation pattern` in OpenSees is then introduced. Three typical examples involving extreme behaviors and/or complex stress state are presented as they demonstrate the superior of the explicit methods in overcoming non-convergence. Meanwhile, the key algorithmic parameters are analyzed to investigate their influence on the results, and setting recommendations are made for practical applications.

2. Unconditionally stable explicit dynamic integration method

Without loss of generality, the dynamic motion equation of a multi-DOF structure can be written as

$$\mathbf{M}\ddot{\mathbf{u}}(t) + \mathbf{C}\dot{\mathbf{u}}(t) + \mathbf{R}[\mathbf{u}(t), \dot{\mathbf{u}}(t)] = \mathbf{F}(t) \tag{1}$$

where $\mathbf{M}$ and $\mathbf{C}$ are the mass and damping matrices, respectively; $\mathbf{u}(t)$, $\dot{\mathbf{u}}(t)$, $\ddot{\mathbf{u}}(t)$ are the displacement, velocity and acceleration vectors of the dynamic system; $\mathbf{R}(t)$ is the resisting force vector, which is usually related to structural displacement and velocity; $\mathbf{F}(t)$ is the applied external force vector; and, t is the time.

To solve the equations of motion, a discrete scheme is needed. In the KR-α method [24], the equations are transformed into the following form by constructing the corresponding updating equations for velocity and displacement as follows:

$$\mathbf{M}\widehat{\ddot{\mathbf{X}}}_{i+1} + \mathbf{C}\dot{\mathbf{X}}_{i+1-\alpha_f} + \mathbf{R}_{i+1-\alpha_f} = \mathbf{F}_{i+1-\alpha_f} \tag{2}$$

with

$$\begin{aligned} \dot{\mathbf{X}}_{i+1} &= \dot{\mathbf{X}}_i + \boldsymbol{\alpha}_1 \Delta t \ddot{\mathbf{X}}_i \\ \mathbf{X}_{i+1} &= \mathbf{X}_i + \Delta t \dot{\mathbf{X}}_i + \boldsymbol{\alpha}_2 \Delta t^2 \ddot{\mathbf{X}}_i \end{aligned} \tag{3}$$

in which $\mathbf{X}_i, \dot{\mathbf{X}}_i, \ddot{\mathbf{X}}_i$ represent the displacement, velocity and acceleration vectors at the ith time step, respectively; Δt is the time step size; $\boldsymbol{\alpha}_1$ and $\boldsymbol{\alpha}_2$ are two integration parameter matrices; and, $\widehat{\ddot{\mathbf{X}}}_{i+1}$, $\mathbf{X}_{i+1-\alpha_f}$, $\mathbf{R}_{i+1-\alpha_f}$, and $\mathbf{F}_{i+1-\alpha_f}$ are the intermediate acceleration, velocity, resisting force and applied force vectors, respectively, which are defined as follows:

$$\begin{aligned} \widehat{\ddot{\mathbf{X}}}_{i+1} &= (\mathbf{I} - \boldsymbol{\alpha}_3)\ddot{\mathbf{X}}_{i+1} + \boldsymbol{\alpha}_3 \ddot{\mathbf{X}}_i \\ \dot{\mathbf{X}}_{i+1-\alpha_f} &= (1-\alpha_f)\ddot{\mathbf{X}}_{i+1} + \alpha_f \ddot{\mathbf{X}}_i \\ \mathbf{R}_{i+1-\alpha_f} &= (1-\alpha_f)\mathbf{R}_{i+1} + \alpha_f \mathbf{R}_i \\ \mathbf{F}_{i+1-\alpha_f} &= (1-\alpha_f)\mathbf{F}_{i+1} + \alpha_f \mathbf{F}_i \end{aligned} \tag{4}$$

where $\mathbf{I}$ is the identity matrix; $\boldsymbol{\alpha}_3$ is an integration parameter matrix; α_f is a scalar integration parameter; and, $\mathbf{R}_i$ and $\mathbf{F}_i$ are the resisting force and applied force vectors at the ith time step, respectively.

To obtain the integration matrices and parameters, the eigenvalues of the amplification matrix of the KR-α method are set equal to that of the generalized-α method [15], and then the integration parameter matrices are determined as follows:

$$\begin{aligned} &\boldsymbol{\alpha}_1 = \left(\mathbf{M} + \gamma \Delta t \mathbf{C} + \beta \Delta t^2 \mathbf{K}_0\right)^{-1} \mathbf{M}, \quad \boldsymbol{\alpha}_2 = \left(\frac{1}{2} + \gamma\right)\boldsymbol{\alpha}_1 \\ &\boldsymbol{\alpha}_3 = \left(\mathbf{M} + \gamma \Delta t \mathbf{C} + \beta \Delta t^2 \mathbf{K}_0\right)^{-1} \left(\alpha_m \mathbf{M} + \alpha_f \gamma \Delta t \mathbf{C} + \alpha_f \beta \Delta t^2 \mathbf{K}_0\right) \end{aligned} \tag{5}$$

where $\mathbf{K}_0$ is the initial stiffness matrix; and, parameters γ, β, α_m and α_f are functions of the high-frequency spectral radius ρ_∞, given below in Eq. (6).

$$\begin{aligned} &\gamma = \frac{1}{2} - \alpha_m + \alpha_f, \quad \beta = \frac{1}{4}(1 - \alpha_m + \alpha_f)^2, \\ &\alpha_m = \frac{2\rho_\infty - 1}{\rho_\infty + 1}, \quad \alpha_f = \frac{\rho_\infty}{\rho_\infty + 1} \end{aligned} \tag{6}$$

It can be seen that the spectral radius ρ_∞ is the only user-defined parameter in the KR-α method. ρ_∞ is associated with the numerical energy dissipation capacity of the algorithm and is in the range of [0, 1]. $\rho_\infty = 1$ means no numerical energy dissipation, where $\rho_\infty = 0$ indicates the maximum numerical energy dissipation. The specific value of ρ_∞ should be determined by the problem and the time step size. The developer [30] recommended that the users should start with $\rho_\infty = 1$ and then gradually reduce ρ_∞ until a stable response is achieved. It should also be noted that too much numerical energy dissipation will influence the response of lower modes of interest, and therefore ρ_∞ should be selected with care.

The KR-α method is implemented in OpenSees by the co-authors, and the command lines are provided in Appendix A. Note that a nonsingular mass matrix must be adopted when the KR-α method is used.

3. Finite element modeling for typical RC structures

In order to demonstrate the feasibility of the proposed analysis scheme, the modeling strategy in the OpenSees should be introduced

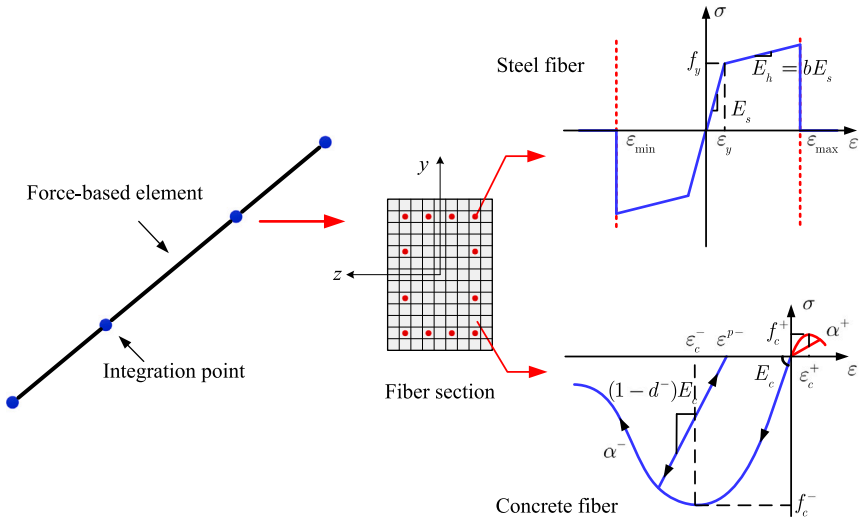

Fig. 1. Fiber beam–column element with nonlinear material.

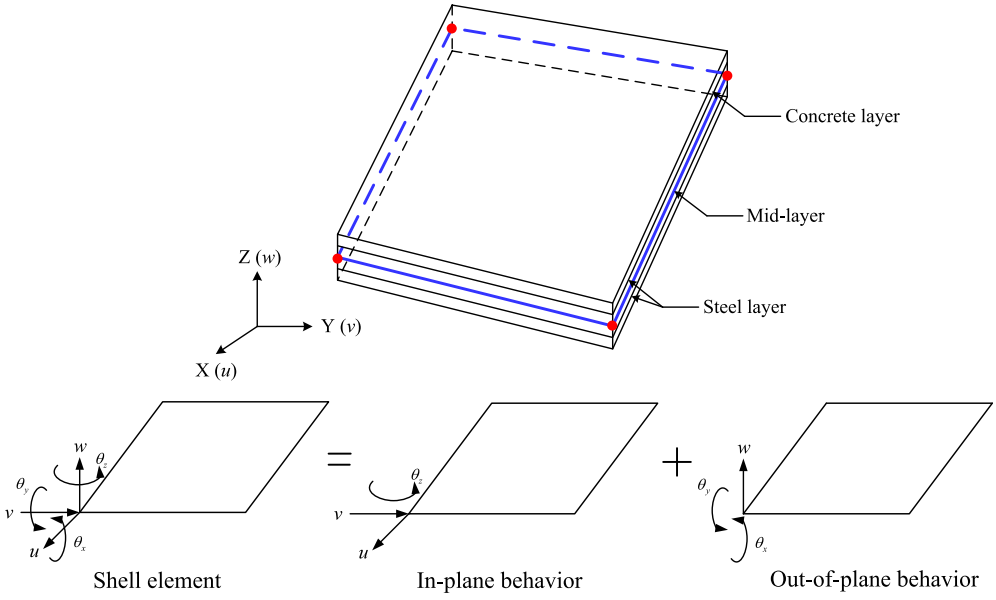

Fig. 2. Multi-layered shell element.

firstly since KR-α method has only been implemented in it. The two types of elements employed in the numerical example parts and modeling strategies for RC components will be briefly introduced here, that is, the force-based fiber beam element for beam-like components and the multi-layer shell element for wall-like components.

3.1. Force-based fiber beam elements

In OpenSees, the force-based beam element with fiber section is usually employed to model beam/column members in structures, as shown in Fig. 1. It usually has better performance than the displacement-based element since it strictly satisfies equilibrium at the element level even in the highly nonlinear phase. Therefore, a more coarse mesh can be used in the simulation, e.g., one element with four Gauss–Lobatto integration points is sufficient to model each beam/column member [32,33]. The section of the element is divided into several fibers and different stress–strain relations are assigned to different fibers to model materials (e.g., concrete and steel). Many options are available for material models in OpenSees, for example, the bilinear stress–strain model Steel01 with isotropic hardening effect for reinforcement bars and the plastic-damage mechanics-based model concreteD [34] for concrete. The steel models are often used with Min–Max criterion in order to reflect the reinforcement fracture [13,35]. Besides, the confinement effect provided by transverse reinforcement can be well-simulated by modifying the material parameters of core concrete fibers based on the Mander's model [36,37].

3.2. Multi-layered shell element

For wall-type structures, the multi-layered shell element is usually adopted for simulation as it can reflect the in-plane and out-of-plane behaviors of the walls. The element formulation is implemented in OpenSees using the four-node "ShellMITC4" element, which is divided into a number of layers of different thickness as indicated in Fig. 2, and each layer is assigned with different material properties. For concrete, multi-dimensional constitutive model is required to represent the multi-dimensional behavior, while for reinforcement steel, they are assumed to be smeared over the layer according to the reinforcing ratio and their principal directions, and Menegotto and Pinto model [38] is often adopted to simulate the behaviors of the steel bars.

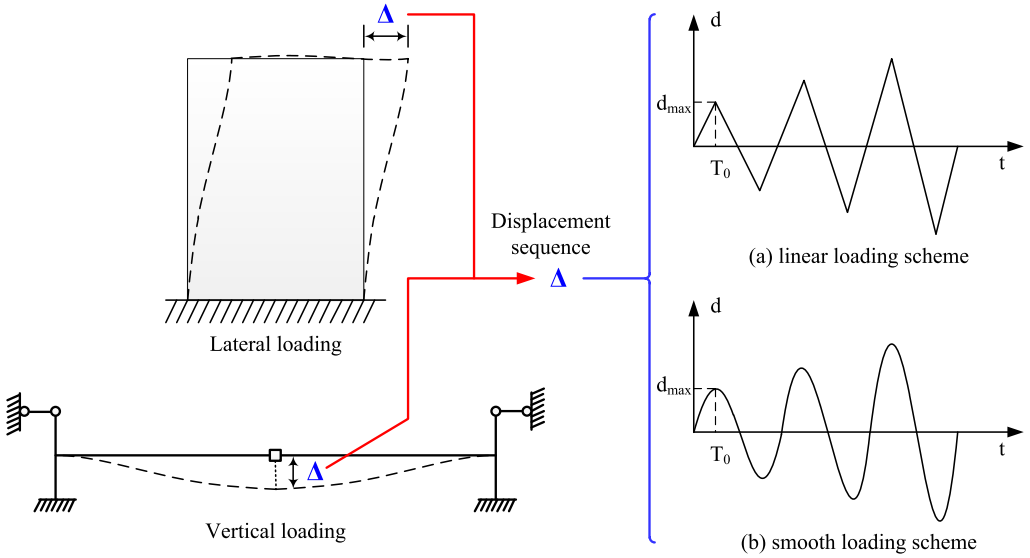

Fig. 3. Dynamic application of static displacements for structural analysis.

In the multi-layer shell element, the axial strains and curvature of the middle layer are firstly calculated, and the strains of other layers are then computed according to the plane-section assumption. By calling for the material constitutive laws, the stress resultants and stiffness matrix can be obtained through integrating over each layer. The element is proven to be an effective way that can well simulate the coupled in-plane/out-of-plane bending as well as the in-plane direct shear and coupled bending/shear behavior of the RC shear walls [39].

4. Static loading scheme in dynamic analysis procedure

In traditional static analysis, external excitation is applied through a force-control scheme or a displacement-control scheme. In most cases, the displacement-control scheme is preferred, because it can predict the limit capacity and capture the structural behaviors under decreasing process more accurately. In the displacement-control scheme, target displacements are given to specific nodes, such as the top node of a shear wall or the middle node of a beam as shown in Fig. 3, and then the reaction of the system can be obtained for further analysis. An iteration technique is usually employed to reach the target displacement, and convergence issues may be encountered in this process.

However, in a dynamic analysis in OpenSees, external excitation is applied using the `Uniform Excitation Pattern` or the `Multi-Support Excitation Pattern`. For example, in a seismic analysis, a ground motion is applied to the supports (base nodes of the model) using one of these patterns. It is not straightforward to directly impose static displacements at structural nodes. In this regard, the paper develops a loading scheme to apply the displacement at any nodes in the dynamic analysis in OpenSees.

The `Multi-Support Excitation Pattern` is employed to apply the static displacements. `The Multi-Support Excitation Pattern` in OpenSees allows similar or different prescribed ground motions to be input at various supports in the structure. Unlike the `Uniform Excitation Pattern` in which the prescribed ground motions should be acceleration sequences and applied to the support (base nodes) only, the `Multi-Support Excitation Pattern` also allows displacement sequences with a target value as the prescribed ground motions in the dynamic analysis. Therefore, displacement sequences are used as the inputs to the 'supports'–the nodes where the loads need to be applied, as shown in Fig. 3.

Different displacement sequences represent different loading schemes, some of which may induce considerable dynamic effects. In this paper, two typical loading schemes are studied. One is a linear loading scheme shown in Fig. 3(a). It should be noted that cyclic loads can be regarded as a combination of several monotonic loads, and the linear loading scheme can be expressed as follows for the kth monotonic load:

$$d(t) = d_{ini,k} + \frac{t - T_{ini,k}}{T_{end,k} - T_{ini,k}} \cdot (d_{end,k} - d_{ini,k}) \tag{7}$$

where $d(t)$ represents the displacement at time t; $T_{ini,k}$ and $T_{end,k}$ are the initial time and end time of the kth monotonic load, respectively; $d_{ini,k}$ and $d_{end,k}$ are the initial displacement and target displacement of the kth monotonic load, respectively; $t = T_{ini,k} + n \cdot dt,\ n = 1, 2 \ldots N_{step,k}$; dt is the time interval in the generated displacement sequence, and $N_{step,k} = (T_{end,k} - T_{ini,k})/dt$ is the number of loading step in the kth monotonic load.

The other is a smooth loading scheme shown in Fig. 3(b), which is expressed as [6]:

$$d(t) = d_{ini,k} + \left[1 + \cos\left(\frac{t - T_{ini,k}}{T_{end,k} - T_{ini,k}} \cdot \pi + \pi\right)\right] \cdot (d_{end,k} - d_{ini,k})/2 \tag{8}$$

The meaning of parameters in Eq. (8) are the same as those in Eq. (7). In addition, in a pure monotonic loading case, i.e., $d_{ini,k} = 0$, $d_{end,k} = d_{max}$, $T_{ini,k} = 0$ and $T_{end,k} = T_0$, where T_0 is the total time of loading and d_{max} is the target displacement as show in Fig. 3, then Eqs. (7) and (8) are reduced to

$$d(t) = \begin{cases} t/T_0 \cdot d_{max} & \text{for linear loading} \\ \left[1 + \cos\left(t/T_0 \cdot \pi + \pi\right)\right] \cdot d_{max}/2 & \text{for smooth loading} \end{cases} \tag{9}$$

It should be noted that there are many ways to produce the displacement sequences, but the object of this paper is not to find the best one but to propose a feasible way to overcome the convergence issues, thus only these two loading schemes are studied.

A typical command line for applying the nodal displacement at a selected node using the `Multi-Support Excitation Pattern` is provided in Appendix B.

5. Numerical examples

In this section, three numerical examples in total are presented to illustrate the effectiveness and advantages of the explicit dynamic approach in solving the static extreme behavior of structural components and systems. The first two examples are at component level while the third one is at structural level. Among the three examples, examples

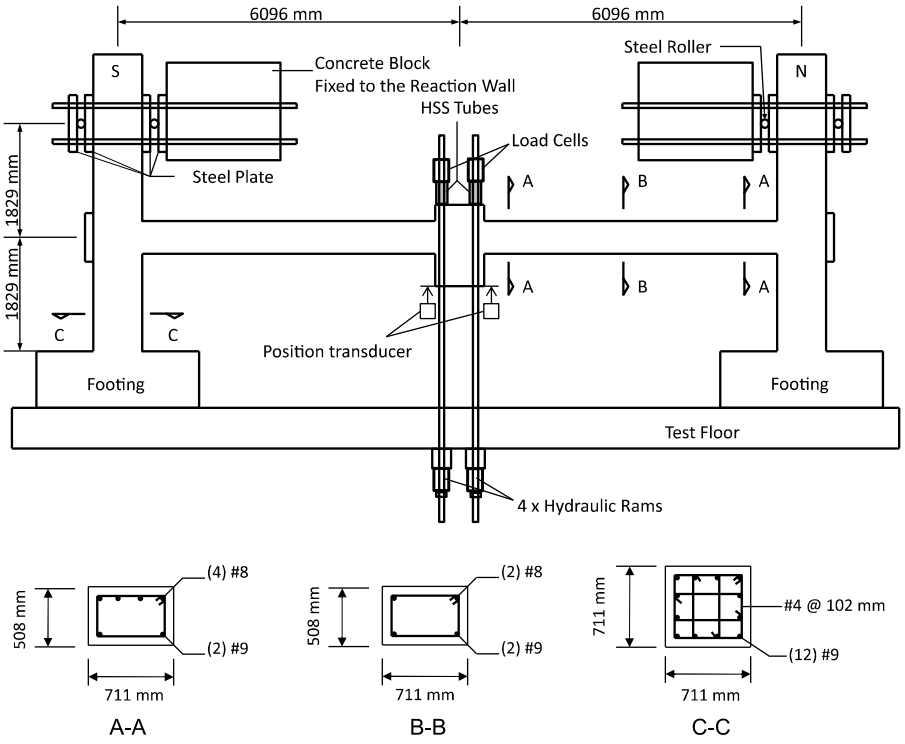

Fig. 4. Details of the column removal test on RC sub-assemblage by Lew et al. [40].

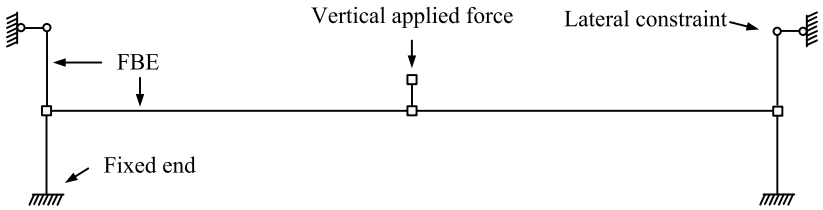

Fig. 5. Schematic of the FE model.

1 and 3 are RC structures under progressive collapse since this failure involves both material and geometric nonlinearities, example 2 is a RC shear wall under cyclic lateral displacement which produces significant shear effect, so all three examples are with typical extreme behavior and/or complex stress states.

5.1. RC sub-assemblage under column removal

The first example is a column removal analysis of an RC sub-assemblage. The experiment is conducted by Lew et al. [40]. As shown in Fig. 4, the beam span is 6069 mm with a section of 508 mm× 711 mm. The figure also gives the reinforcing details for the specimen. The compressive strength of the concrete is 32 MPa. As for reinforcement, the yielding strength and the fracture strain for the No. 8 bars are 476 MPa and 21%, respectively, while they are 462 MPa and 18% for No. 9 bars, respectively. More details about the experiment can be found in the original reference.

Fig. 5 gives the schematic of the finite element (FE) model. Each beam is simulated by one force-based fiber element with the ConcreteD constitutive model for concrete and Hysteretic Material models for steels. The columns are fixed with the floor, and springs are used to simulate the constraints at the top of the columns. Besides, a density of 2500 kg/m^3 is used to calculate the lumped masses, and the first-order vibration period of the system is 0.07 s (s).

Both static and dynamic approaches are adopted for comparison. In the static approach, the vertical displacement of 1100 mm is imposed directly at the middle column node using displacement-control scheme, and the Newton–Raphson algorithm is used as the solution method. The displacement increment is set as 0.1 mm, and the convergence tolerance is set as 10^{-6} on the energy norm. In the dynamic approach, the KR-α method is used and the smooth loading scheme is selected to generate the displacement sequence. The total time of loading is set as $T_0 = 1$ s; the time interval in the generated excitation is set as $dt = 0.01$ s. The analysis time step size is set as $\Delta t = 0.007$ s, which is about 1/10 of the first-order vibration period. Rayleigh proportional damping based on mass and tangent stiffness corresponding to 5% of critical damping in the first and third modes is used.

Figs. 6(a) and 6(b) present the comparisons of the experimental and numerical load–displacement curves of the specimen in both the vertical and horizontal directions, respectively. A typical resistance force curve of RC sub-assemblage under column-removal scenario can be divided into three stage. In the beginning, the behaviors of the beams are similar to three-point bending, called the beam stage. After that, cracks occur in the bottom of the middle section and the top of the beam-end, resulting in the compressive arch action (CAA) and reaching the first peak in Fig. 6(a). With load increasing, concrete is crushed and the load is mainly resisted by the reinforcement, and this is called the tensile catenary action (TCA). The second peak in Fig. 6(a) represents the capacity of the TCA, and the structure fails after the second peak. It is seen that the numerical results are in good agreement with the experimental ones, for both the static and dynamic approaches. The actual CAA capacity by the test is 296.2 kN, while predicted CAA

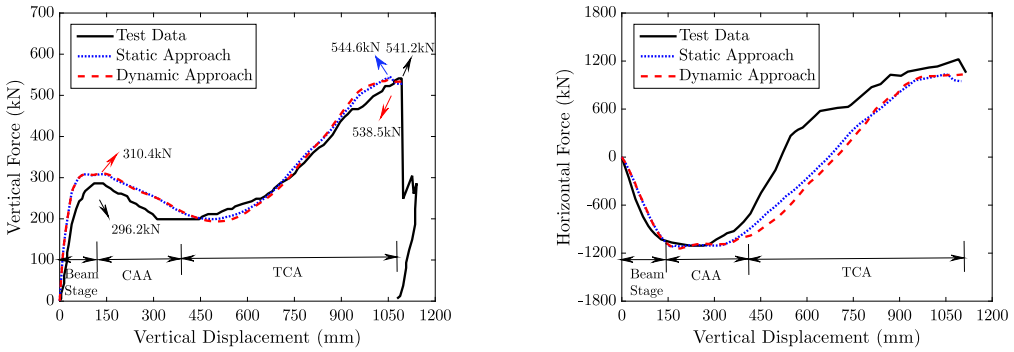

(a) Vertical load-displacement curve

(b) Horizontal load-displacement curve

Fig. 6. Load–displacement curves of the RC sub-assemblage under column removal scenario.

capacity by static and dynamic approaches are the same, 310.4 kN, with an error of 4.79%. For TCA capacity, experimental result is 541.2 kN and the calculated one is 544.6 kN in the static approach and 538.5kN in the dynamic approach. The errors for the two approaches are 0.63% and −0.5%, respectively, which indicates that both the static and dynamic approaches can predict the TCA capacity well. Similarly, for the horizontal resistance force, the dynamic approach also shows the same accuracy as the static one. Thus, it is fair to say that the proposed dynamic approach can effectively model the column-removal scenario.

5.2. RC shear wall under cyclic lateral load

For better validation of the proposed method, a numerical example of shear wall under cyclic lateral load is also presented here. The shear wall specimen RW-A20-P10-S38 that is presented in the Ph.D. dissertation by Tran [41] is employed. As shown in Fig. 7(a), the specimen is 152.4 mm in thickness and 1219.2 mm in width, with lateral load applied at 2438.4 mm above the wall-foundation block interface, which means the wall's aspect ratio is only 2.0. The axial load level of the specimen is $0.1A_g f_c$, where A_g is the cross-sectional area of the wall and f_c is the specified concrete compressive strength.

Evidently, the wall is a typical squat wall so it will have obvious shear effect. The finite element model is established based on the multi-layered shell mentioned before. Totally 32 shell elements is employed in the model, as shown in Fig. 7(b). The wall foundation is fixed with the floor. The Menegotto and Pinto model is used to describe the behaviors of the reinforcing steel bars, and the multi-dimension concrete model in OpenSees is used to describe the behaviors of the concrete. The compressive strength of the concrete is 47.1 MPa, and the tensile strength is set as 2.0 MPa. The yield strength of ϕ6.35, ϕ9.53 and ϕ12.7 steel bars are 423 MPa, 472 Mpa and 450 MPa, respectively. A density of 2500 kg/m^3 is adopted to calculate the lumped masses, and the first-order vibration period of the system is 0.065 s.

Four ways are adopted to simulate the shear wall for comparisons, first is the traditional static approach, second we used the implicit Newmark-β dynamic approach with Newton–Krylov algorithm to enhance the convergence performance, third one we used explicit dynamic approach with CDM, and last one is the explicit KR-α dynamic approach, i.e, the proposed approach. In the static approach, displacement-control scheme is employed with the Newton–Raphson algorithm. The displacement step size is 0.01 mm and the convergence tolerance is set as 10^{-5} on energy norm. In the dynamic approach, the total loading time T_0 is set as T_0=10 s, and the time interval in the displacement excitation is set as dt=0.005 s. For implicit Newmark-β method, a convergence tolerance of 10^{-5} on the energy norm and a maximum number 800 of iteration is employed, and the analysis time step is set as Δt=0.001 s. For explicit CDM, the analysis time step is set as $\Delta t = 5 \times 10^{-7}$s. For explicit KR-$\alpha$ method, $\rho_\infty = 0.8$ is employed according to the procedure mentioned in Section 2, and the analysis time step is set as Δt=0.001 s. Furthermore, Rayleigh damping ratio proportional to mass and tangent stiffness is set as 0.05.

Fig. 8 gives the lateral displacement–load curves that are obtained through the three approaches. It can be seen that the traditional static approach diverges at an early stage, thus it is impossible to obtain the limit capacity of the shear wall. Dynamic approach with Newmark-β algorithm has a better performance than the traditional static approach but still encounters with divergence issue. Dynamic approach with CDM will not encounter convergence issues in theory. However it can be seen from Fig. 8(c) that even though a extreme small analysis time step of 5×10^{-7}s is adopted, the stability requirement of CDM is not satisfied thus no reliable structural responses is obtained. By contrast, the dynamic approach with the KR-α method can simulate the structural response by adopting a much larger analysis time step and therefore is much more efficient than the dynamic approach with traditional CDM. It can predict the whole process accurately without any divergence issue, thus sufficient data can be acquired for further performance assessment of the shear wall.

5.3. RC frame under progressive collapse

The performance of the proposed dynamic approach is demonstrated at the component-level modeling examples above. Here a structural-level is also studied to show the feasibility of the proposed method. A five-story planar RC frame is designed in accordance with the Chinese design code [42]. The frame is assumed to be located in Nanjing, China, where the seismic intensity is VII, which means the peak ground acceleration that is used for designing structures is 0.1 gal with a 10% exceedance probability in 50 years. The geometric dimensions and the reinforcing details are given in Fig. 9. The dead load is 5 kN/m^2 for the floor and 7 kN/m^2 for the roof, while the live load is 2 kN/m^2 for both floor and roof. The concrete compressive strength is 20 MPa and reinforcement elastic modulus, yielding strength and hardening ratio are 2×10^5 MPa, 400 MPa and 0.01, respectively.

The gravity loads are combined as 1.2×dead load+0.5×live load according to [43] and then applied to the structure. Two scenarios of pushdown analysis are performed, one is the removal of interior column B and the other is the removal of the exterior column A. The target pushdown displacement of the removed column node is determined through the collapse criterion in [43] as follows: if the vertical displacement of the node exceeds 1/5 of the shortest span of the connecting beams, the structure fails. Thus, the target vertical displacement is determined as 1200 mm. Four approaches that are mentioned in the last shear wall example are adopted to solve the problem for comparisons.

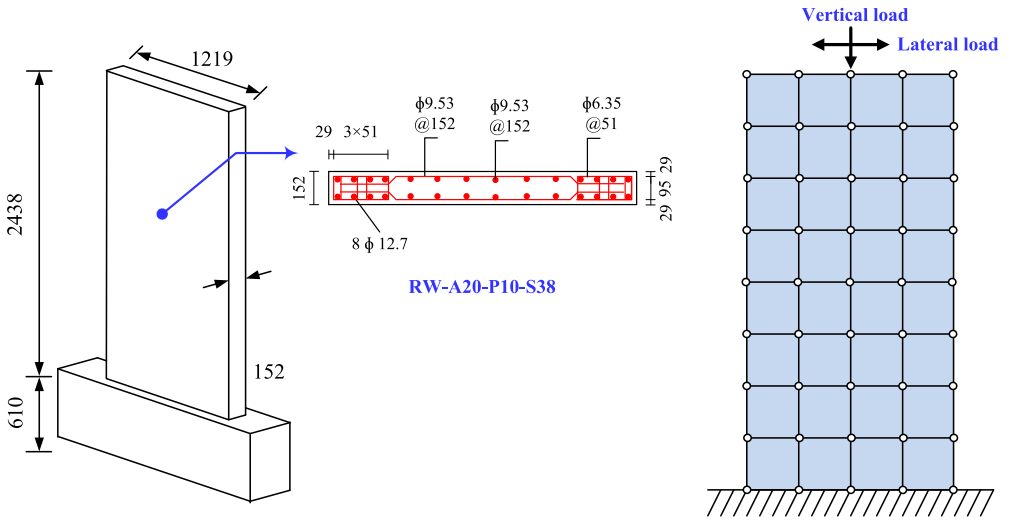

(a) Schematic of the shear wall specimen (b) Schematic of the Finite Element model

Fig. 7. Schematic of the shear wall specimen by Tran [41] and the corresponding FE model.

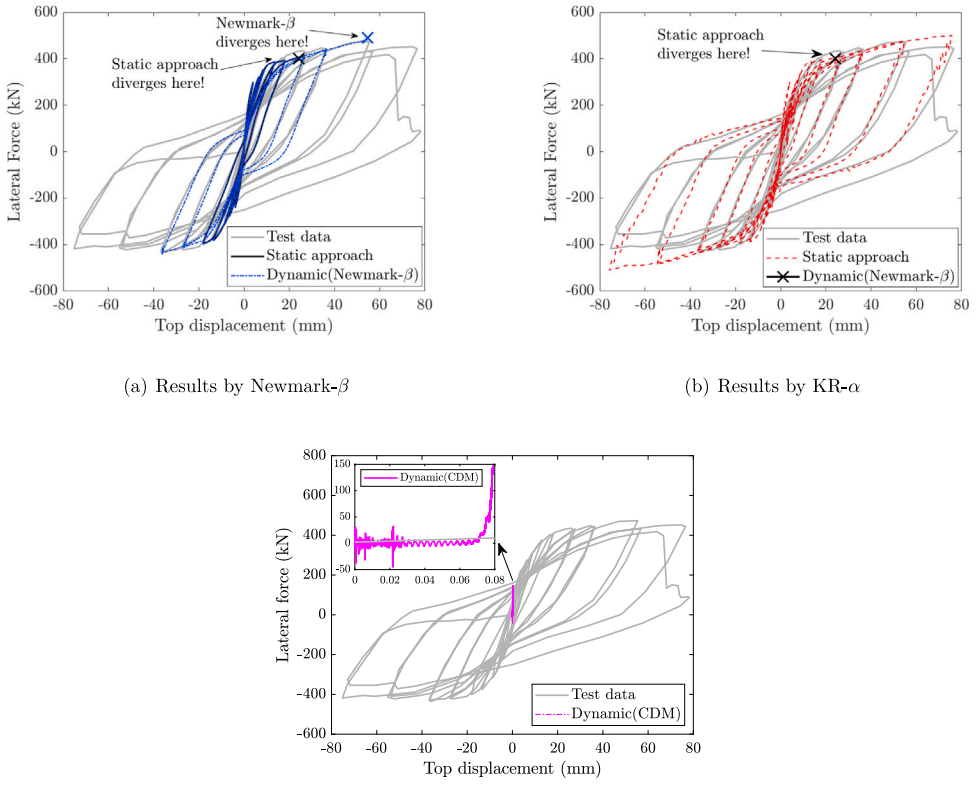

(a) Results by Newmark-β (b) Results by KR-α

(c) Results by CDM

Fig. 8. Load–displacement curve of the shear wall under cyclic lateral load.

The first-order natural vibration period of the RC frame is 0.935 s. For the static approach, the displacement increment is set as 0.1 mm, and the tolerance for convergence is set as 10^{-6} on the energy norm. For the dynamic approaches, the total loading time is set as T_0=10 s with time interval dt = 0.02s. The Rayleigh damping ratio proportional to mass and tangent stiffness is 0.05. Furthermore, for the implicit Newmark-β algorithm, a convergence tolerance of 10^{-6} on the energy norm and a maximum number 200 of iterations is employed, and the analysis time step is set as Δt=0.005 s. For the explicit CDM, the analysis time step is set as $\Delta t = 5 \times 10^{-6}$s. For the explicit KR-$\alpha$ algorithm, ρ_∞ = 0.5 is used according to the procedure mentioned in Section 2, and the analysis time step is set as Δt=0.005 s.

Fig. 10 shows the results for the two column removal scenarios, i.e exterior column removal and interior column removal. The vertical resistance forces of the remaining structure is plotted against the vertical displacement. It can be found that the pushdown curves have three typical stages: (1) the load is mainly resisted by the beam-end moments, and the total resistance force increases with the displacement; (2) the

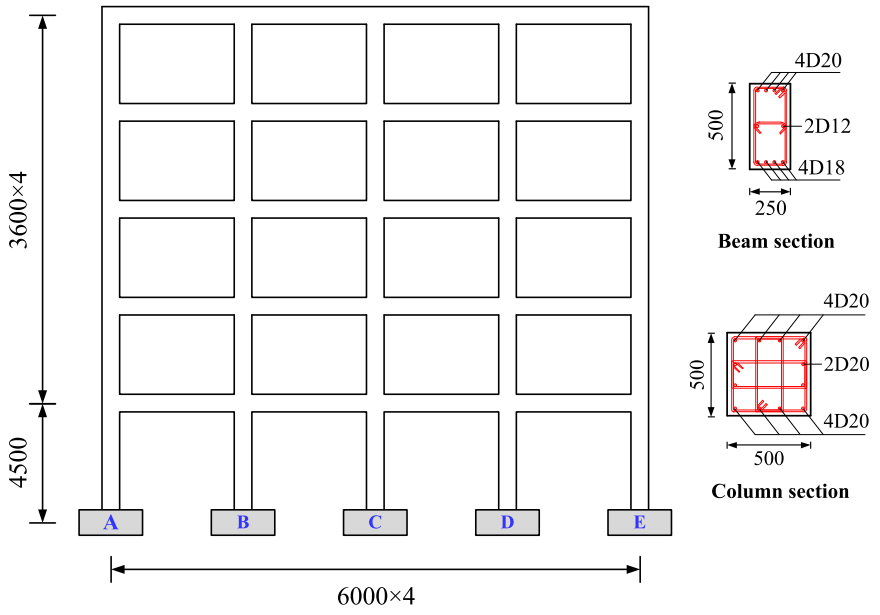

Fig. 9. Layout of the five-story planar RC frame.

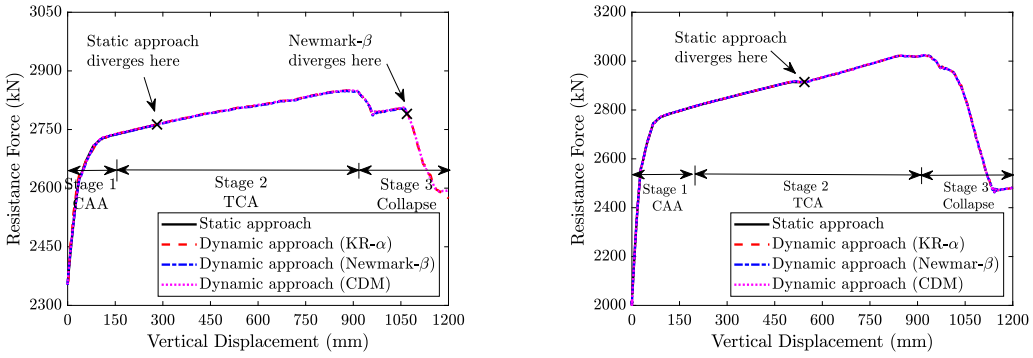

(a) Removal of exterior column A (b) Removal of interior column B

Fig. 10. Pushdown curves for the frame under different column removal scenarios.

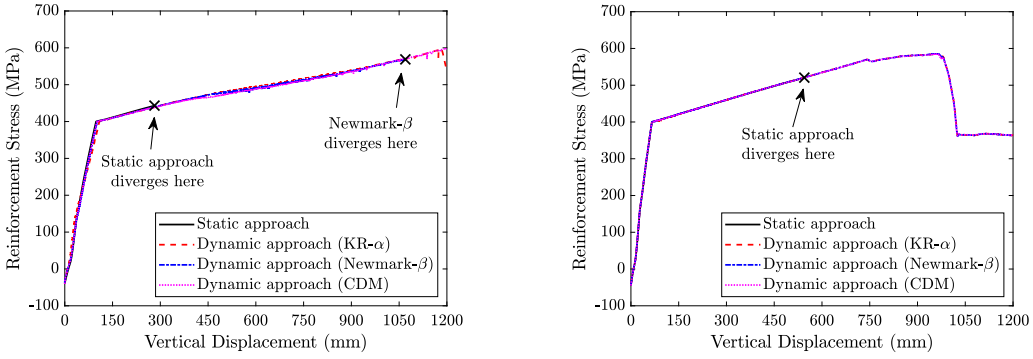

(a) Removal of exterior column A (b) Removal of interior column B

Fig. 11. Stresses of the reinforcement under different column removal scenarios.

plastic hinges are fully developed at the beam ends, the state of sections of the beam transfers from compression to tension, causing the TCA, which continues to improve the capacity; (3) the longitudinal rebars fracture as the vertical displacement continues to increase, leading to a drop of the curves, indicating the failure of the structure. The static analysis approach encounters a convergence problem in the second

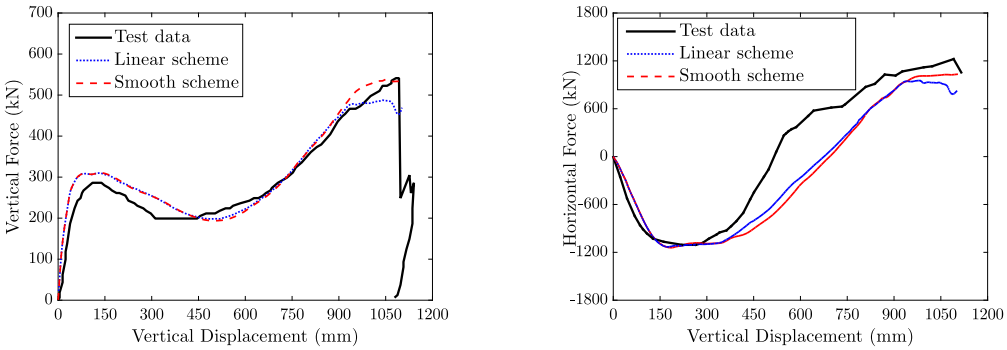

(a) Vertical load-displacement curve

(b) Horizontal load-displacement curve

Fig. 12. Effect of loading scheme.

stage and stops before it reaches the maximum capacity (the second peak value), for both scenarios. For the implicit dynamic approach with Newmark-β algorithm, it can capture the whole process of the interior column removal scenario, but for the exterior column removal scenario, it can only obtain the behavior of the structure before the occurrence of the second rebar fracture. Two explicit dynamic approaches perform well for both removal scenario. Fig. 11 gives the stresses of the reinforcements located in the bottom of the middle of the damaged span. It proves that the proposed method can obtained responses as accurately as the traditional CDM from both global level and local level with a much large analysis step size.

Overall, the explicit dynamic approach with the KR-α method can attain the entire collapse behavior for both scenarios, exhibiting a obvious superiority in the pushdown analysis (extreme behavior modeling) without any convergence problem.

6. Factors affecting the accuracy of the dynamic approach

Though the effectiveness of the proposed dynamic method is proved through the simulations of the above examples, there are many parameters in the dynamic algorithm settings, e.g., the loading scheme, the total loading time, the time interval in the displacement excitation, the analysis step size, and the damping ratio, etc., that can effect the result. To this end, a parametric analysis is performed on the first example (i.e., the RC sub-assemblage under column removal) to investigate the influence of these factors on the result for better understanding and application of the proposed approach. The reference values for the parameters are set as follows unless otherwise specified: (1) smooth loading scheme with a prescribed displacement of 1100 mm at the loading points; (2) total loading time $T_0 = 1$ s; (3) the time interval of the displacement excitation $dt = 0.01$ s; (4) analysis time step size $\Delta t = 0.007$ s; and (5) damping ratio $\xi = 0.05$.

The effect of the loading scheme is firstly studied and the simulated results by the smooth loading scheme and linear loading scheme are indicated in Fig. 12. As shown in the figure, the results of the two loading schemes are almost the same, but the smooth loading scheme can predict the TCA capacity more accurately than the linear loading scheme, since the smooth loading scheme uses a more gentle way to apply the displacement in the final stage. Thus the smooth loading scheme is recommended in the dynamic approach. Fig. 13 shows the effect of the total loading time on the displacement–load curves. The total loading time determines the speed of applying the displacement. It can be found that a too short total loading time will lead to an inaccurate simulation, since a considerable dynamic effect may be induced. It can also be observed that a too long loading time can result in an underestimation of the TCA. Thus, choosing a proper loading time is necessary, and it is recommended to set it to a small value (e.g., 1 s) firstly and then prolong it step by step until the dynamic effect disappears.

Fig. 14 shows the effect of the time interval dt in the displacement excitation, which seems to have no effect on the simulation. In other words, the ratio $dt/\Delta t$ may not influence the performance of the dynamic approach. Fig. 15 shows the effect of the analysis time step size. In traditional seismic analyses, the analysis time step size should be smaller than the time interval dt in the earthquake record as well as 1/10 of the system's first-order natural vibration period T_1. Here five different ratios (i.e. $\Delta t/T_1$=1, 1/2, 1/10, 1/20, 1/50) are investigated. As can be seen from the figure, an accurate prediction cannot be obtained when the ratio $\Delta t/T_1$ is large than 1/10, and there is no obvious difference between the three predictions when the ratio $\Delta t/T_1$ is less than 1/10. Thus, the analysis step size Δt is recommended to be less than 1/10 of the system's first-order natural vibration period T_1. Fig. 16 displays the effect of damping ratio on the simulation, and the damping ratio seems to have no effect on the simulation.

7. Concluding remarks

This paper presents a dynamic approach to simulate static structural extreme behaviors by using the explicit KR-alpha method which is implanted in OpenSees by the co-authors. Compared with traditional explicit algorithms requiring a small analysis time step for stability, the KR-α algorithm is unconditionally stable and allows analysis adopting a large analysis time step. The `Multi-Support Excitation Pattern` in OpenSees is used to apply the static loadings dynamically, and three numerical examples are employed to demonstrate the advantages of the proposed method over the traditional static analysis, dynamic approach with implicit algorithms, and dynamic approach with conditionally stable explicit algorithms. A parametrical study is also conducted to investigate the effect of different parameter settings, and recommendations for the parameter settings are given. Based on the results, the following collusion can be drawn.

(1) Static analysis involving high nonlinearity can be conducted in a dynamic way with the KR-α method, and the responses obtained through the proposed approach exhibit the same accuracy as other approaches from both global level and local level;
(2) Compared with the traditional static approach and the dynamic approach with implicit Newmark-β algorithm, the proposed method can overcome the convergence issue when simulating extreme structural behaviors.
(3) The CDM will not encounter convergence issues in theory. However, it requires a small, even unacceptable step size to maintain stability. Compared with the dynamic approach with CDM, the proposed method can overcome the convergence issues with a

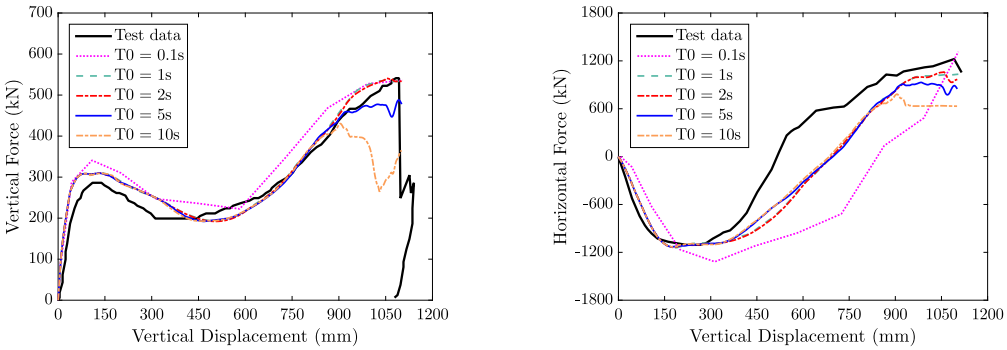

(a) Vertical load-displacement curve (b) Horizontal load-displacement curve

Fig. 13. Effect of total loading time.

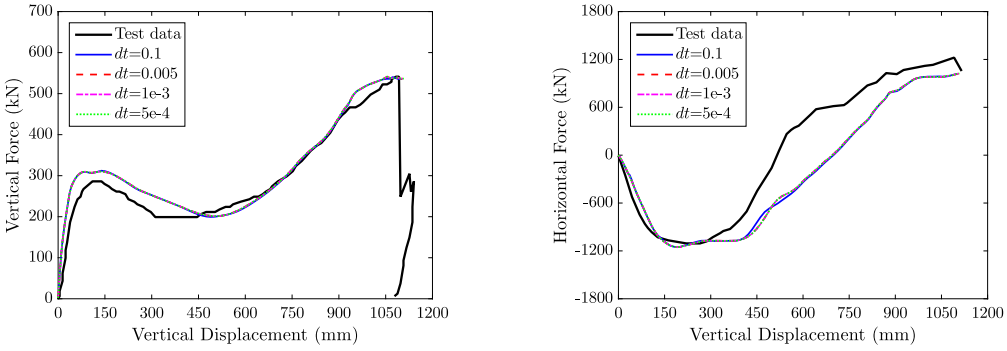

(a) Vertical load-displacement curve (b) Horizontal load-displacement curve

Fig. 14. Effect of the time interval in the generated displacement excitation.

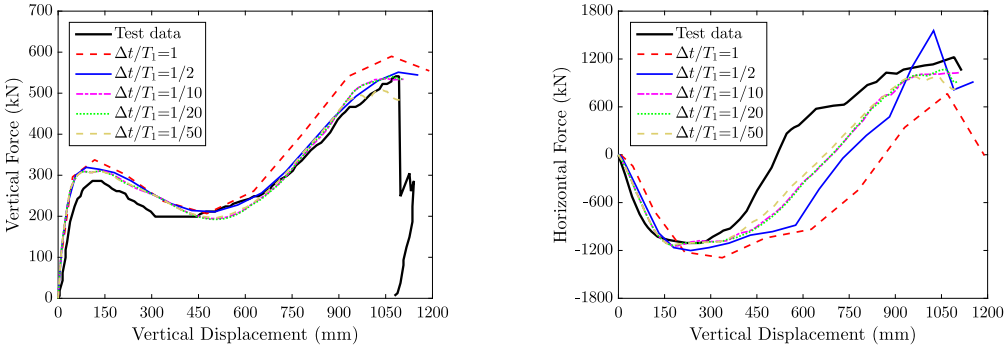

(a) Vertical load-displacement curve (b) Horizontal load-displacement curve

Fig. 15. Effect of time step size.

much larger time step size. The proposed method owns the same accuracy but is much more efficient than the dynamic approach with the CDM.

(4) The results of the parametrical analysis show that the time interval dt in the generated excitation and the damping ratio ξ seems to have no effect on the performance of the proposed dynamic approach; both smooth and linear loading scheme can simulate the extreme behavior efficiently and accurately, but the smooth one is more recommended; the total loading time T_0 is recommended to set a small value (e.g., 1 s) at first, and then prolong it until the dynamic effect disappear; the analysis time step size Δt should be less than 1/10 of the system's first-order vibration period.

Declaration of competing interest

The authors declare that they have no known competing financial interests or personal relationships that could have appeared to influence the work reported in this paper.

Acknowledgments

The authors greatly appreciate the financial support from the Project of National Key Research and Development Program of China (Grant No. 2022YFC3803004), the National Natural Science Foundation of China (Grant No. 52078119), and the Natural Science Foundation of Jiangsu Province (Grant No. BK20211564).

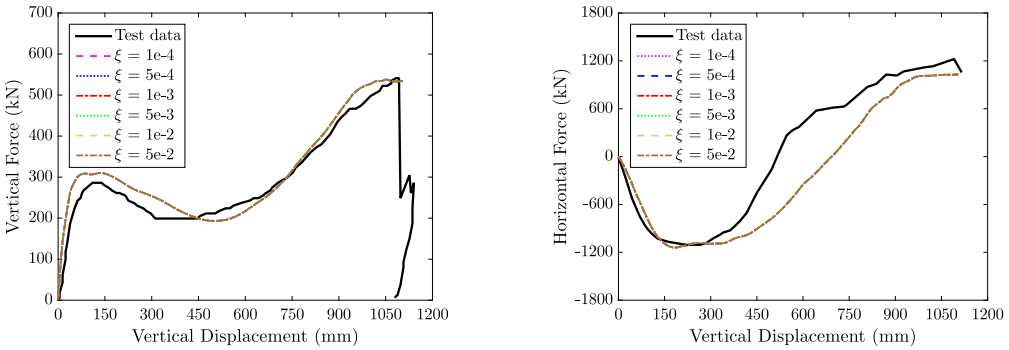

(a) Vertical load-displacement curve

(b) Horizontal load-displacement curve

Fig. 16. Effect of damping ratio.

Appendix A. Code lines for KR-α method

The command lines for employing the KR-α method in OpenSees are provided as follows:

- `integrator KRAlphaExplicit $`ρ_∞
- `algorithm Linear`
- `system FullGeneral`
- `analysis Transient`

where `$`ρ_∞ represents the value of the high-frequency spectral radius which is mentioned in Section 2.

Appendix B. Code lines for applying the nodal displacement

A typical command line for applying the nodal displacement at a selected node using the `Multi-Support Excitation Pattern` is given as follows:

```
pattern MultipleSupport $patternTag {
    groundMotion $gMotionTag Plain -disp $tsTag;
    imposedMotion $nodeTag $dirn $gMotionTag; }
```

where `groundMotion` and `imposedMotion` are respectively used to generate a ground motion and apply it to the structural model; `$gMotionTag` is the tag of the predefined ground motion, which is a displacement-type sequence indicated by `-disp`; `$tsTag` is the tag of displacement sequence generated by Eqs. 7 or 8; `$nodeTag` is the tag of the node where the displacement should be imposed; `$dirn` is the target DOF of the node along with the displacement is imposed. More details can be found in the user's manual of OpenSees.

References

[1] Riks E, Rankin CC, Brogan FA. On the solution of mode jumping phenomena in thin-walled shell structures. Comput Methods Appl Mech Engrg 1996;136(1):59–92.

[2] Zienkiewicz OC, Taylor RL. The finite element method for solid and structural mechanics. London: Butterworth-Heinemann; 2005.

[3] Scott MH, Fenves GL. Krylov subspace accelerated Newton algorithm: Application to dynamic progressive collapse simulation of frames. J Struct Eng 2010;136(5):473–80.

[4] Ren X, Li J. Two-level consistent secant operators for cyclic loading of structures. J Eng Mech 2018;144(8).

[5] Feng D-C, Ren X-D, Li J. Softened damage-plasticity model for analysis of cracked reinforced concrete structures. J Struct Eng 2018;144(6).

[6] Chen G, Teng J, Chen J, Xiao Q. Finite element modeling of debonding failures in FRP-strengthened RC beams: A dynamic approach. Comput Struct 2015;158:167–83.

[7] Crisfield M. Non-linear finite element analysis of solids and structures. In: Essentials, vol. 1. Chichester:England: John Wiley & Sons Ltd.; 1991.

[8] Yu R, Ruiz G. Static multi-crack modeling in concrete solved by a modified DR method. Comput Concrete 2004;1(4):371–88.

[9] Yu R, Ruiz G. Explicit finite element modeling of static crack propagation in reinforced concrete. Int J Fract 2006;141(3–4):357–72.

[10] Dhanasekar M, Haider W. Explicit finite element analysis of lightly reinforced masonry shear walls. Comput Struct 2008;86(1):15–26.

[11] Nasiri E, Liu Y. Development of a detailed 3D FE model for analysis of the in-plane behaviour of masonry infilled concrete frames. Eng Struct 2017;143:603–16.

[12] Earij A, Alfano G, Cashell K, Zhou X. Nonlinear three-dimensional finite-element modelling of reinforced-concrete beams: Computational challenges and experimental validation. Eng Fail Anal 2017;82:92–115.

[13] Feng D, Kolay C, Ricles JM, Li J. Collapse simulation of reinforced concrete frame structures. Struct Des Tall Special Build 2016;25(12):578–601.

[14] Newmark NM. A method for computation for structural dynamics. J Eng Mech Div 1959;85.

[15] Chung J, Hulbert G. A time integration algorithm for structural dynamics with improved numerical dissipation - The generalized-alpha method. J Appl Mech-Trans ASME 1993;60(2):371–5.

[16] Chang S. Explicit pseudodynamic algorithm with unconditional stability. J Eng Mech 2002;128(9):935–47.

[17] Chen C, Ricles JM. Development of direct integration algorithms for structural dynamics using discrete control theory. J Eng Mech 2008;134(8):676–83.

[18] Fu B, Zhang F-T. A dual-explicit model-based integration algorithm with higher-order accuracy for structural dynamics. Appl Math Model 2022;110:513–41.

[19] Chang S-Y. Discussion of paper 'real-time hybrid testing using the unconditionally stable explicit CR integration algorithm' by Cheng Chen, James M. Ricles, Thomas M. Marullo and Oya Mercan, Earthquake Engineering and Structural Dynamics 2009; 38:23-44. Earthq Eng Struct Dynam 2012;41(5):1061–3.

[20] Noh G, Bathe K-J. An explicit time integration scheme for the analysis of wave propagations. Comput Struct 2013;129:178–93.

[21] Bathe K-J, Baig MMI. On a composite implicit time integration procedure for nonlinear dynamics. Comput Struct 2005;83(31–32):2513–24.

[22] Bathe K-J. Conserving energy and momentum in nonlinear dynamics: A simple implicit time integration scheme. Comput Struct 2007;85(7):437–45.

[23] Noh G, Bathe K-J. The bathe time integration method with controllable spectral radius: The ρ_∞-Bathe method. Comput Struct 2019;212:299–310.

[24] Kolay C, Ricles JM. Development of a family of unconditionally stable explicit direct integration algorithms with controllable numerical energy dissipation. Earthq Eng Struct Dynam 2014;43(9):1361–80.

[25] Kolay C, Ricles JM. Improved explicit integration algorithms for structural dynamic analysis with unconditional stability and controllable numerical dissipation. J Earthq Eng 2019;23(5):771–92.

[26] Qing LC, Li Zhong J. Unconditionally stable explicit displacement method for analyzing nonlinear structural dynamics problems. J Eng Mech 2018;144(9).

[27] Chang S-Y. A dual family of dissipative structure-dependent integration methods for structural nonlinear dynamics. Nonlinear Dynam 2019;98(1):703–34.

[28] Tang Y, Ren D, Qin H, Luo C. New family of explicit structure-dependent integration algorithms with controllable numerical dispersion. J Eng Mech 2021;147(3).

[29] Feng D-C, Wang Z, Wu G. Progressive collapse performance analysis of precast reinforced concrete structures. Struct Des Tall Special Build 2019;28(5):e1588.

[30] Kolay C, Ricles JM, Marullo TM, Mahvashmohammadi A, Sause R. Implementation and application of the unconditionally stable explicit parametrically dissipative KR-alpha method for real-time hybrid simulation. Earthq Eng Struct Dynam 2015;44(5):735–55.

[31] McKenna F, Fenves GL, Scott MH, et al. Open system for earthquake engineering simulation. Berkeley, CA: University of California; 2000.

[32] Scott M, Fenves G. Plastic hinge integration methods for force-based beam-column elements. J Struct Eng 2006;132(2):244–52.

[33] Feng D-C, Xie S-C, Xu J, Qian K. Robustness quantification of reinforced concrete structures subjected to progressive collapse via the probability density evolution method. Eng Struct 2020;202.
[34] Wu JY, Li J, Faria R. An energy release rate-based plastic-damage model for concrete. Int J Solids Struct 2006;43(3):583–612.
[35] Lu X, Lu X, Guan H, Ye L. Collapse simulation of reinforced concrete high-rise building induced by extreme earthquakes. Earthq Eng Struct Dynam 2013;42(5):705–23.
[36] Mander J, Priestley M, Park R. Theoretical stress-strain model for confined concrete. J Struct Eng 1988;114(8):1804–26.
[37] Feng D-C, Ding Z-D. A new confined concrete model considering the strain gradient effect for RC columns under eccentric loading. Mag Concr Res 2018;70(23):1189–204.
[38] Filippou FC, Popov EP, Bertero VV. Effects of bond deterioration on hysteretic behavior of reinforced concrete joints. Earthquake Engineering Research Center, University of California Berkeley; 1983.
[39] Lu X, Xie L, Guan H, Huang Y, Lu X. A shear wall element for nonlinear seismic analysis of super-tall buildings using OpenSees. Finite Elem Anal Des 2015;98:14–25.
[40] Lew HS, Bao Y, Sadek F, Main JA, Pujol S, Sozen MA. An experimental and computational study of reinforced concrete assemblies under a column removal scenario. NIST Technical Note 2011;1720:106.
[41] Tran TA. Experimental and analytical studies of moderate aspect ratio reinforced concrete structural walls (Ph.D. thesis), UCLA; 2012.
[42] Ministry of Housing and Urban Rural Development of the People's Republic of China, Beijing. Code for design of concrete structures. Beijing, China; 2010.
[43] DoD. Unified facilities criteria:Design of structures to resist progressive collapse. Washington, DC: US Department of Defense; 2010.